Oxidation of Metals, Vol. 4, No. 3, 1972

The High-Temperature Oxidation of Iron–Chromium–Nickel Alloys Containing 0–30% Chromium*

J. E. Croll† and G. R. Wallwork‡

Received July 26, 1971—Revised March 22, 1972

The oxidation behavior of iron–chromium–nickel alloys containing 0–30% chromium has been determined for oxidation at 1000°C in static pure oxygen atmospheres. Particular emphasis has been placed on the correlation between the kinetics of oxidation and the morphologies and compositions of the scales produced. Maximum oxidation resistance was associated with the formation of chromic oxide scales on alloys containing greater than 20% chromium. The loss of an oxide species from these scales by volatilization may limit the usefulness of alloys protected by chromic oxide scales to a temperature less than 1000°C.

INTRODUCTION

In an earlier publication[1] the alloy compositional ranges of iron–chromium–nickel alloys which gave rise to completely chromic oxide scales were determined for an oxidation temperature of 1000°C. This paper gives details of the oxidation kinetics and the metallography, x-ray diffraction and electron proble microanalysis of the oxidized specimens for alloys containing up to 30 wt.% chromium.§

The oxidation kinetics and the morphology of the scales produced during oxidation of iron–chromium alloys have been the subject of numerous papers in recent years[2–9] and have been reviewed in considerable detail by

* Research supported by the Broken Hill Proprietary Co., Ltd., Postgraduate Research Scholarship.

† Australian Iron and Steel Pty. Ltd., Port Kembla, Australia.

‡ School of Metallurgy, University of New South Wales, Kensington, Australia.

§ Unless otherwise specified, all compositions referred to in this paper are in weight percent.

Table I

Alloy	Nominal composition (wt. %)			Actual composition (wt. %)		
	Cr	Ni	Fe	Cr	Ni	Fe
FF	—	5	95	—	4.9	95.1
GG	—	30	70	—	30.2	69.8
HH	—	55	45	—	55.0	45.0
JJ	—	85	15	—	82.3	17.7
W	2	60	38	2.4	59.1	38.5
A	5	5	90	5.8	5.1	89.1
Q	5	15	80	5.7	15.1	78.8
BB	5	40	55	5.1	40.3	54.6
T	5	50	45	5.4	48.5	46.1
CC	5	70	25	5.2	69.8	25.0
N	5	90	5	5.7	89.0	5.3
Y	7	93	—	7.2	92.8	—
L	10	15	75	10.6	15.7	73.7
R	10	50	40	9.9	48.4	41.7
V	10	60	30	10.2	59.6	30.2
P	10	80	10	10.7	78.7	10.6
X	12	88	—	12.1	87.9	—
G	15	30	55	15.3	30.3	54.4
J	15	40	45	14.6	38.9	46.5
S	15	50	35	15.1	49.8	35.1
U	15	60	25	15.3	59.5	25.2
B	20	5	75	18.9	5.5	75.6
DD	20	25	55	19.4	24.7	55.9
EE	20	65	15	20.2	64.6	15.2
AA	20	80	—	19.9	80.1	—
E	25	5	70	26.5	4.8	68.7
D	25	15	60	24.0	15.9	60.1
H	25	20	55	24.8	17.3	57.9
Z	25	60	15	24.9	59.6	15.5
F	30	5	65	30.3	3.9	65.8

Table II

Element	Inconel X-750	Inconel 600	Nimonic 75
Cr	16.0	15.85	20.5
Ni	70.6	76.4	77.4
Fe	6.8	7.2	0.5
C	0.05	0.04	0.10
Mn	1.0 max.	0.20	0.45
S	0.01 max.	0.007	0.007
Si	0.50 max.	0.20	0.45
Cu	0.50 max.	0.10	0.05
Ti	2.5	—	0.35
Al	0.9	—	0.15
Nb	0.9	—	—

Wood and his colleagues.[10–13] In general, the iron–chromium–oxygen phase diagram proposed by Seybolt[14] has adequately described the scales formed on iron–chromium alloys by oxidation under kinetic conditions. Wood and Hodgekiess[15] have described the scaling behavior of nickel–chromium alloys and Wood *et al.*[11] have compared this behavior with that observed with iron-chromium alloys. The nickel–chromium–oxygen phase diagram determined by an equilibration method has been published and the oxidation behavior of nickel–chromium alloys related to this diagram.[1] Rapp[16] in a review of the kinetics, microstructure, and mechanism of internal oxidation, described the appearance of this phenomenon in nickel–chromium alloys. The oxidation of iron–nickel alloys has been summarized by Foley[17] and more recently by Wulf *et al.*[18] who interpreted their results in terms of the iron–nickel–oxygen phase diagram.[19,20] The large number of investigations of the oxidation behavior of ternary iron–chromium–nickel alloys and commercial alloys based on this ternary system have been reviewed,[10,21] but few systematic studies of this problem have been undertaken.

EXPERIMENTAL TECHNIQUES

The alloys used in this study were prepared using spectrographically pure nickel (Johnson–Matthey analysis: 7 ppm Fe, 4 ppm Si, 1 ppm Al and Mg, less than 1 ppm Ca, Cu, and Ag), pure iron (Johnson–Matthey analysis: less than 15 ppm total metallic impurities), and pure electrolytic chromium (D.S.L. Melbourne, analysis: less than 20 ppm total metallic impurities, 0.009% oxygen). They were prepared by levitation melting and inert-gas arc melting, the ultimate homogeneity of the specimens being confirmed by subsequent electron probe microanalysis, using an ARL-EMX Mark II electron probe microanalyzer operated at 25 KV. In addition, several commercial nickel-based alloys were examined for purposes of comparison with the ternary alloys. The bulk compositions of the ternary alloys are given in Table I, while those of the commercial alloys are given in Table II.

The alloys were cold rolled to a thickness of 3 mm, cut into rectangular specimens approximately 1 cm × 1.5 cm, and provided with a hole for suspension in the furnace. Metallographic polishing to a 280-mesh SiC surface finish was followed by an anneal at 1000°C for 1 hr in vacua of about 10^{-4} Torr, and then repolishing from 280 mesh through to a 0–1 μ diamond paste finish.

The specimens for thermogravimetric determinations were suspended within a silica reaction tube from a Cahn RG Electrobalance in a dried oxygen atmosphere (medical grade) at a pressure of 200 Torr. The specimens for metallographic examination were suspended up to four at a time within an all-glass system fitted with a silica reaction tube, and exposed to a similar

Table III. Weight Gains After 100 hr Oxidation (mg/cm^2)

Nickel content (wt.%)	Chromium content (wt.%)									
	0	2	5	10	12	15	20	25	30	100
0	460									3.29[a]
5	115		107				3.00	3.45	1.44	
15			84	78				3.72		
20								2.11		
25							1.96			
30	53.5					9.57				
40			28.5			8.53				
50			20.3	13.79		3.47				
55	21.2									
60		13.00		11.50		3.12		2.30		
65							0.82			
70			16.72			3.05[b]				
77						1.18[c]	1.80[d]			
80				7.45			1.38			
85	13.38									
88					13.14					
90			16.05							
100	6.15									

[a] Ref. 23.
[b] Inconel X-750.
[c] Inconel 600.
[d] Nimonic 75.

environment. All specimens were then rapidly brought to the oxidation temperature of 1000 ± 3°C, the temperature being measured by a platinum–platinum–13% rhodium thermocouple, and maintained at this temperature for times ranging from 5 min to 100 hr.

Wherever possible, the specimens which were oxidized principally for metallographic examination were accurately weighed (10^{-6} g) before and after oxidation to provide a further check on the reliability of the weight gain measurements obtained from the Cahn RG Electrobalance (10^{-7} g).

Conventional metallographic techniques, x-ray diffraction analyses, and electron probe microanalyses were used for scale identification and for determinations of the oxide compositions and compositional changes in the alloy beneath the scale.

RESULTS

Typical weight gain curves for the oxidation of the iron–chromium–nickel alloys containing 0–25% chromium are shown in Figs. 1–6. The dashed reference line on each graph ($n = 2$) has a slope equal to that of an ideal parabolic plot. In general the weight gain curves lie approximately parallel to the reference lines on the log-log plots, although many irregularities are apparent. For comparison purposes the average weight gains per unit surface area after 100 hr of oxidation at 1000°C are given in Table III. A more detailed analysis of the kinetics of oxidation of these alloys has been given elsewhere.[22] Nevertheless, it is clear from the comparative data presented in Table III that the oxidation rate depends not only on the chromium content of the alloy but also on the nickel content.

For the given experimental conditions used in this study, good correlation has been obtained between the types of scales produced during oxidation and the resultant rates of oxidation. To facilitate the ensuing discussion, it is convenient to subdivide the alloys into two groups: (a) those that contain less than 20% chromium and so form complex scales, and (b) those that contain 20% chromium or more and form essentially simple scales of chromic oxide.

Fe–Cr–Ni Alloys Containing Less Than 20% Cr

The scales formed during oxidation of the iron-rich alloys in this group consisted of an outer layer of Fe_2O_3 (containing less than 1% Ni and Cr) and an inner layer of iron-rich $Ni_xFe_{(3-x)}O_4$ spinel (containing less than 1% Cr and 1.5 to 20% Ni, depending on the alloy nickel content). An example of such a scale is shown in Fig. 7. These iron-rich alloys exhibited the highest oxidation rates of all the alloys studied, as shown by the iso-oxidation rate curves in Fig. 8. For chromium contents less than about

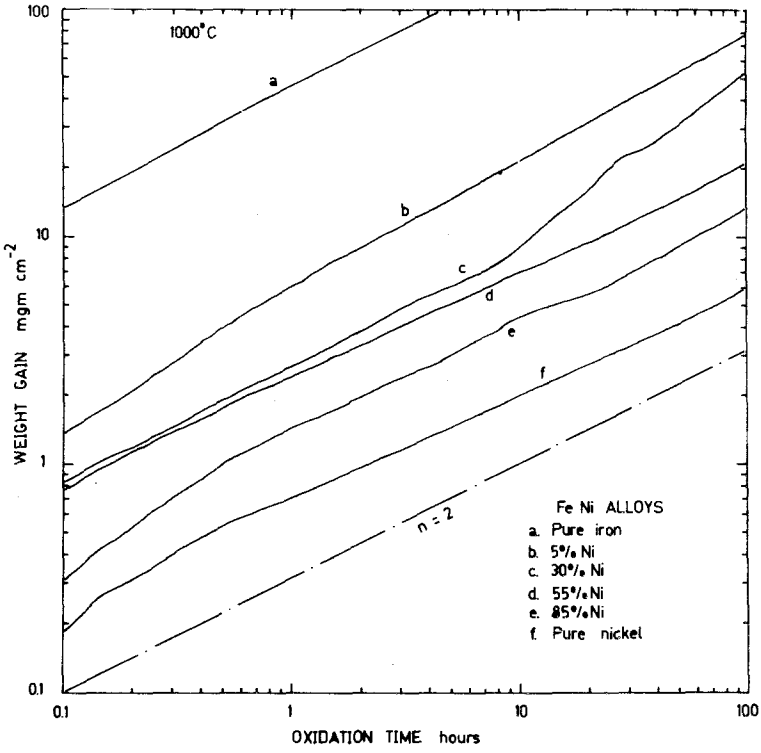

Fig. 1. Weight gain curves for the oxidation of Fe–Ni alloys.

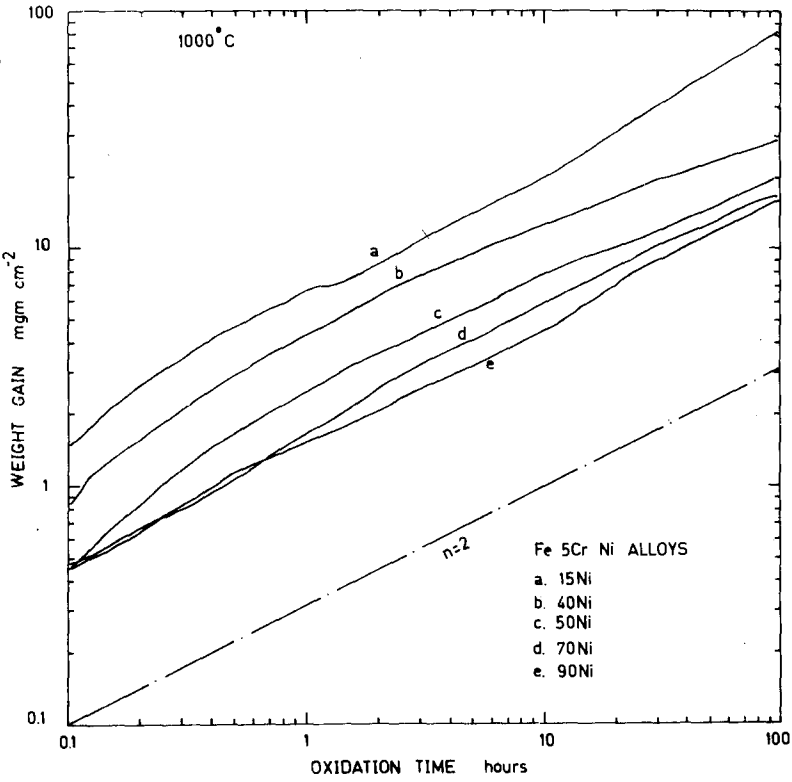

Fig. 2. Weight gain curves for the oxidation of Fe–Ni–5%Cr alloys.

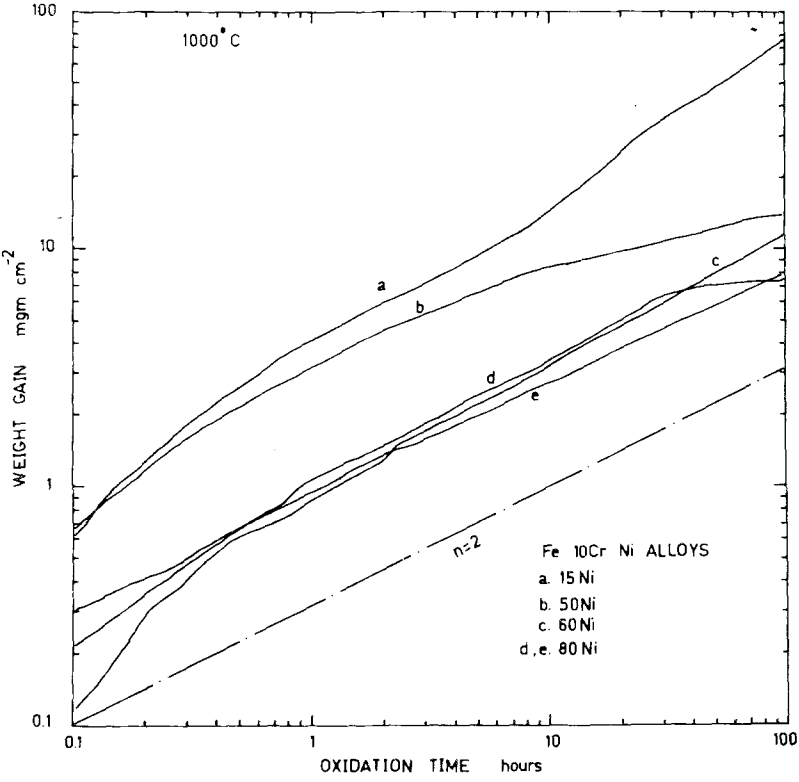

Fig. 3. Weight gain curves for the oxidation of Fe–Ni–10%Cr alloys.

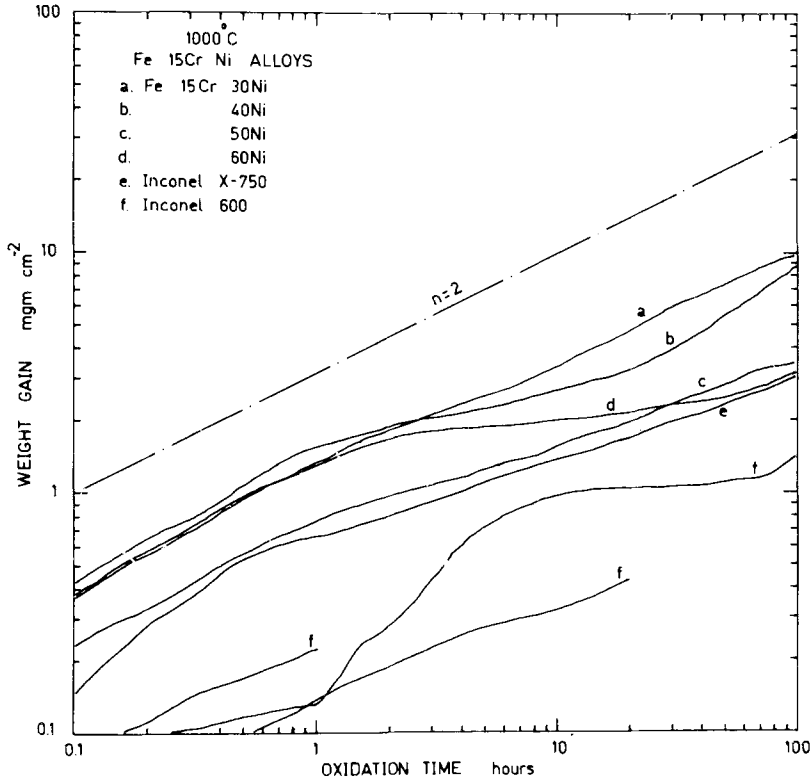

Fig. 4. Weight gain curves for the oxidation of Fe–Ni–15%Cr alloys.

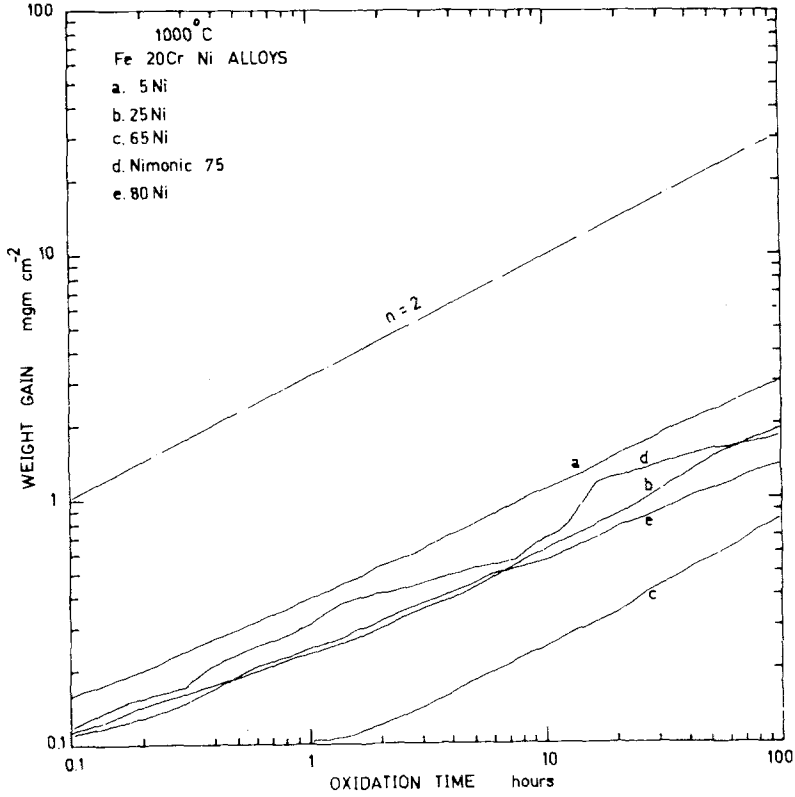

Fig. 5. Weight gain curves for the oxidation of Fe–Ni–20 %Cr alloys.

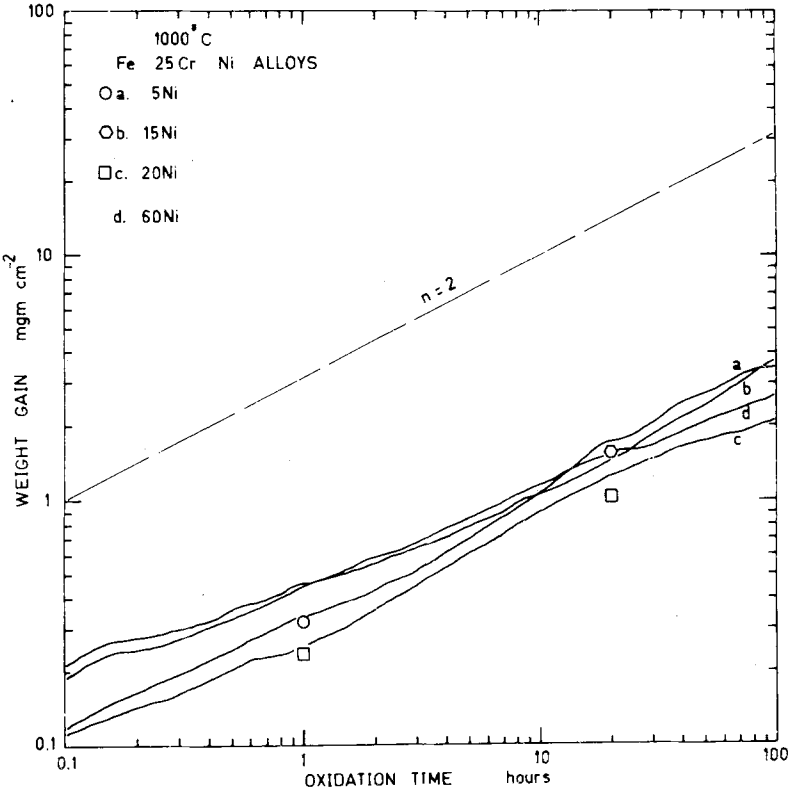

Fig. 6. Weight gain curves for the oxidation of Fe–Ni–25 %Cr alloys.

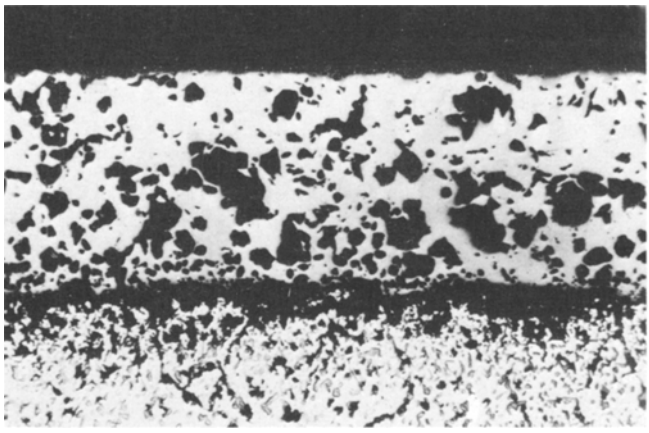

Fig. 7. The external scale and internal oxidation of the Fe–5 %Cr–50 %Ni alloy oxidized for 100 hr. × 250.

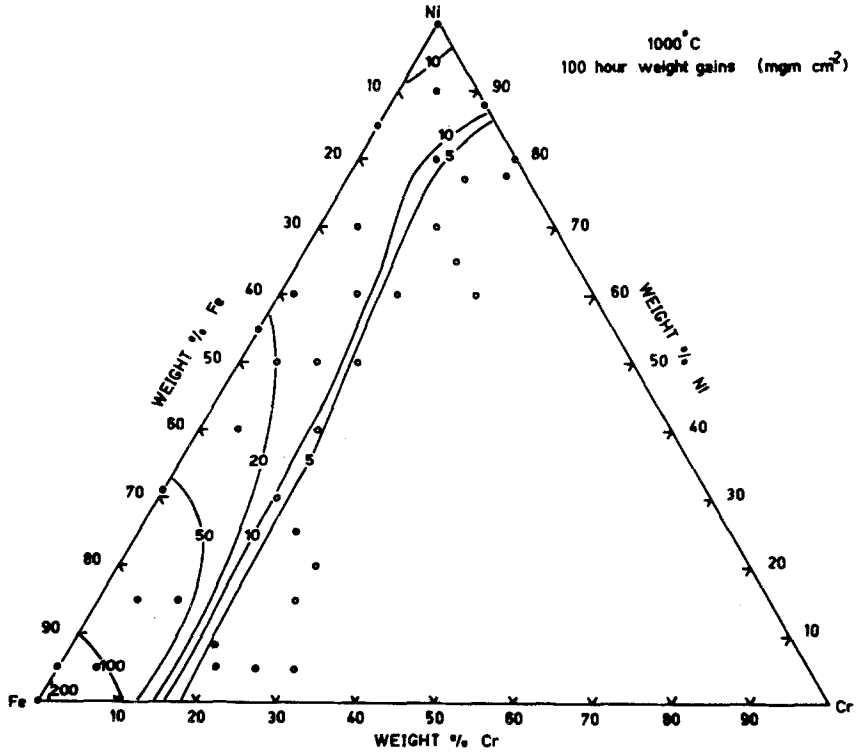

Fig. 8. Isooxidation rate curves for Fe–Cr–Ni alloys (numbers refer to the weight gain in mg/cm^2 after 100 hr. of oxidation at 1000°C).

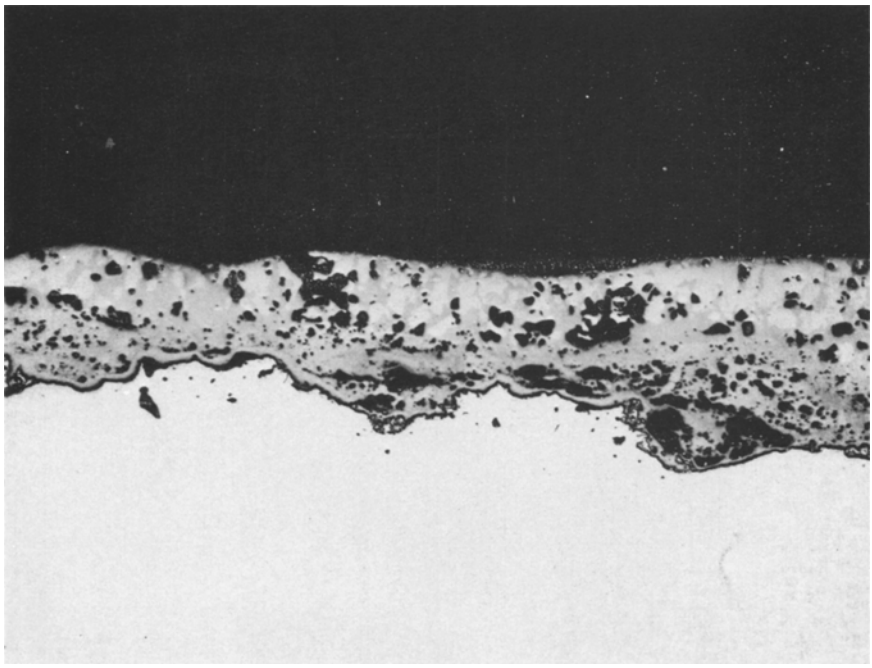

Fig. 9. The external scale, with the inner layer of chromic oxide on the Fe–15%Cr–30%Ni alloy oxidized for 100 hr. × 250.

10% Cr, internal oxidation occurred, with pronounced precipitation in the alloy grain boundary regions particularly. In the alloys containing between 10 and 20% chromium, for which the oxidation rates were lower, a layer of chromic oxide was observed between the remainder of the scale and the alloy after prolonged oxidation (Fig. 9).

The removal of large quantities of iron into the external scale and chromium into the internal oxide particles led to a marked enrichment of nickel in the alloy surface regions, such that concentrations of 80–90% Ni were recorded during electron probe microanalysis of alloys containing 5–40% Ni in the bulk. Nickel concentrations of the order of 80% are sufficiently high to render wustite, FeO, unstable in contact with the alloy,[1] and hence this phase was not observed in the scales of any of the oxidized alloys. For highly iron-rich alloys (less than 2% Ni and 1% Cr), however, the nickel enrichment in the alloy is less than 80% Ni and a wustite layer comprising about 95% of the external scale is observed adjacent to the metal phase.[19] It is the presence of wustite as the major scale component on the very high iron content alloys and pure iron which is responsible for

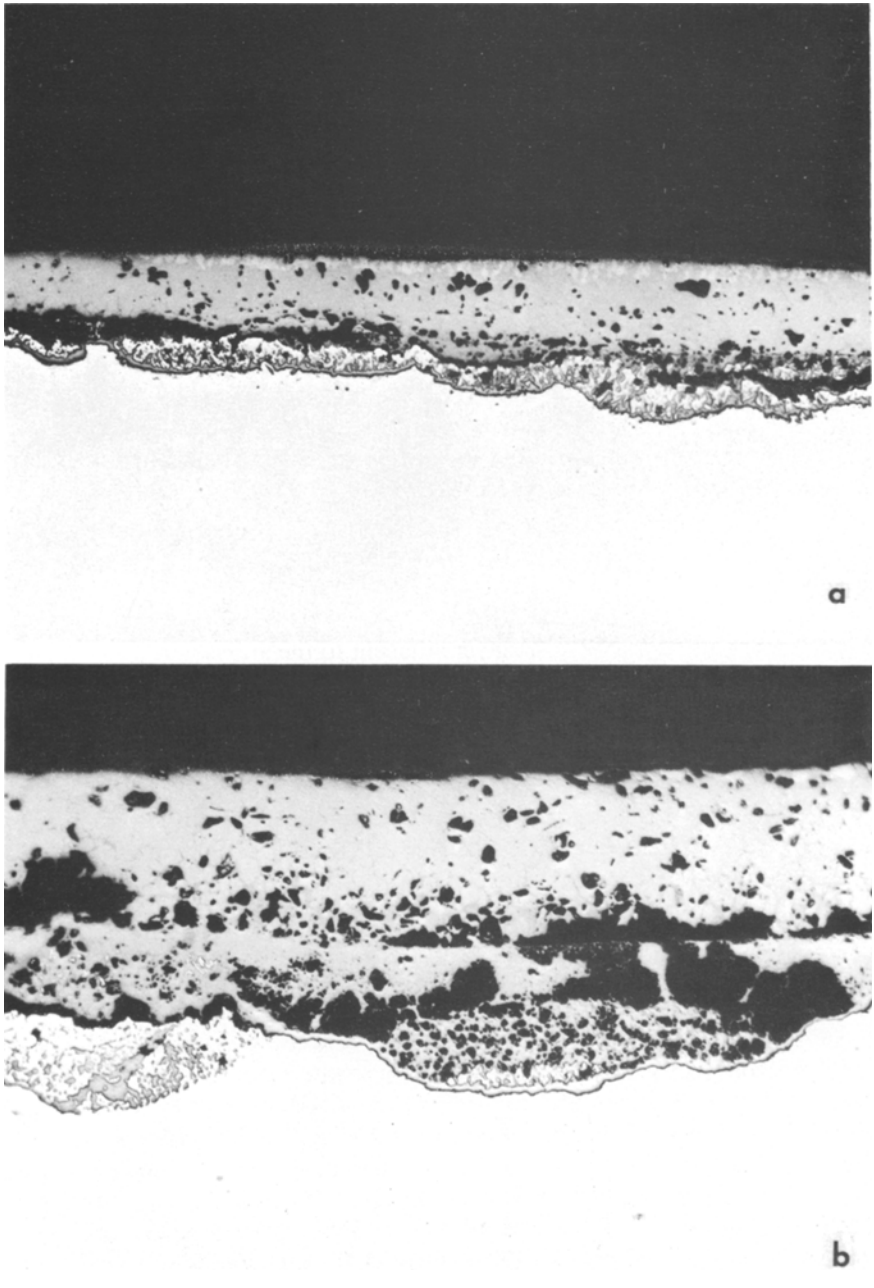

Fig. 10. The scale formed on the Fe–10%Cr–50%Ni alloy by oxidation for (a) 20 hr. × 250. (b) 100 hr. × 250.

their extremely high rates of oxidation. As the nickel content of the alloys is increased above about 2% Ni, the $Ni_xFe_{(3-x)}O_4$ spinel replaces wustite as the major scale layer and the oxidation rates become significantly reduced.

The substitution of more nickel for iron in the alloys at constant chromium contents resulted in further progressive reductions of the oxidation rates. This was due to a series of changes in the constitution of the external scales. As the nickel content of the alloys was increased above about 40% Ni, the spinel phase was essentially stoichiometric $NiFe_2O_4$ (containing 20% Ni and less than 1% Cr). Small "islands" of Fe_2O_3 (containing 1% Ni and less than 0.5 Cr) were distributed toward the outer surface of the spinel phase, the amount of Fe_2O_3 decreasing with higher alloy nickel contents and with longer periods of oxidation (Fig. 10). A further effect of higher nickel contents was the presence of NiO (containing 2–10% Fe and a little Cr) as an inner scale layer after prolonged oxidation. A layer of NiO is apparent between the rest of the external scale and the subscale in Fig. 10(b). Slower cation diffusion rates through the stoichiometric $NiFe_2O_4$ spinel and through the NiO, relative to the diffusion rates through the nickel-deficient $Ni_xFe_{(3-x)}O_4$ spinel on the lower nickel content alloys are responsible for the lower oxidation rates of the higher nickel content alloys. The nickel enrichments in the alloy near the alloy–scale interface were very high and in the range 90–100% Ni whenever NiO was the scale layer adjacent to the alloys.

In common with the iron-based alloys, chromium contents of 10–20% in the nickel-based alloys led to the formation of a compact and fairly continuous layer of chromic oxide at the base of the scale, particularly after prolonged oxidation (Fig. 11). The inner layer of chromic oxide was established faster and more completely as the chromium concentration in the bulk alloy increased.

Fe–Cr–Ni Alloys Containing 20–30% Cr

All the alloys containing 20% chromium or more, as a group had the lowest oxidation rates of all the alloys studied. The rates were generally comparable to or just less than that quoted in the literature for the oxidation of pure chromium.[23] The scales produced during oxidation were very much less complex than those formed on the lower chromium content alloys since chromic oxide was the major component of the scales for all oxidation times up to 100 hr (Fig. 12).

The initial oxide films formed on these alloys contained high iron or nickel concentrations (depending on the relative iron and nickel concentrations in the alloys) as well as chromium. However, owing to the subsequent selective oxidation of chromium, the iron and nickel concentrations in the scale as a whole decreased markedly with time.[22] After prolonged oxidation,

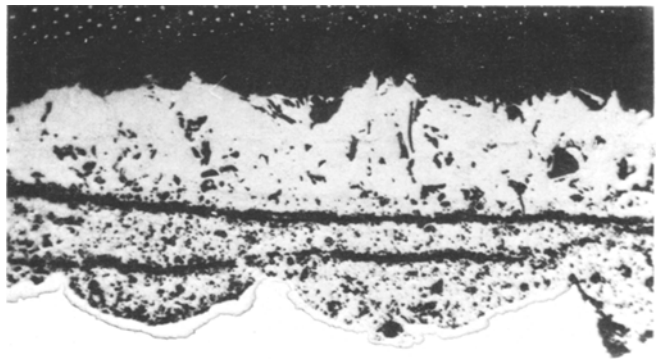

Fig. 11. The scale produced on the Ni–12 %Cr alloy by oxidation for 100 hr. at 1000°C, showing the inner layer of chromic oxide. × 500.

the chromic oxide phase generally contained little or no nickel and less than 2 % iron, with the iron content of the chromic oxide decreasing slightly with increasing chromium content in the alloys. Even after long periods of oxidation, however, high iron concentrations (and occasionally Fe_2O_3) were

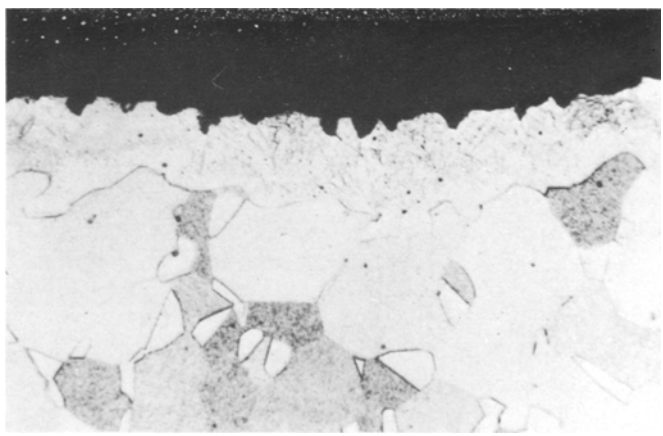

Fig. 12. The chromic oxide scale and ferrite-free rim formed on the Fe–30 %Cr–5 %Ni alloy by 100 hr. of oxidation. × 500.

observed at the outer surface of the scales on the iron-rich alloys as remnants of the nucleation stage. Similarly, nickel-rich oxides and NiO were observed at the external surface of the chromic oxide scale produced on the Nimonic 75 alloy. The failure to observe nickel-containing oxides on the surface of the chromic oxide layer on the other nickel-based alloys was possibly due to these oxides spalling from the chromic oxide layer during cooling of the specimen.

Although internal oxidation of chromium, as such, was absent from these alloys beneath the chromic oxide scales, it was common to observe penetrations of chromic oxide extending from the scale into the alloys along grain and twin boundaries. In the nickel-based alloys these often joined up to form subscale loops and were most probably responsible for the generally better scale adhesion on these alloys.

Iron–chromium–nickel alloys containing in excess of 20% chromium may have a face-centered cubic, body-centered cubic or duplex alloy structure at 1000°C, depending on their particular composition.[24,25] No completely ferritic alloys were studied, although several alloys had the duplex structure. As a result of the depletion of chromium and the corresponding enrichment of iron and nickel in the surface regions during oxidation, a completely ferrite-free layer was formed immediately beneath the external scale (Fig. 12). The thickness of this layer increased with oxidation time, as did the depths of the chromium depletions in the underlying alloys as measured by the electron probe microanalyzer.[22]

When various alloys which owe their protection to chromic oxide scales were oxidized at temperatures of 1000°C and above, negative deviations from ideal parabolic plots were observed[26–28] due to evaporation from the oxide–atmosphere interface of an oxide species. The evaporating species is most probably CrO_3, with the weight loss from the chromic oxide scale occurring by virtue of the reaction:

$$Cr_2O_{3(s)} + \tfrac{3}{2}O_{2(g)} \rightarrow 2CrO_{3(g)}$$

In the present study a thin platinum sheet was suspended in the cooler part of the reaction tube above a sample of each of these alloys in turn; each sample was then oxidized at 1000°C for times up to 100 hr in a static oxygen atmosphere at 200 Torr pressure. Despite this rather crude experimental arrangement, when the platinum sheet was subsequently examined by x-ray diffraction, the presence of a chromic oxide condensate was confirmed in each case. Presumably, if CrO_3 were the evaporating species, then reduction back to Cr_2O_3 occurred in the cooler part of the system.

An analysis of the gravimetric data[22] in terms of the equation:

$$(\Delta W/A) = k_p \times t^{1/2} - k_v \times t$$

Table IV. Comparison of the Experimentally Determined Rate Constants with Those Calculated from Wagner's[29] Analysis and Hagel's[30] Results

Alloy	Vaporization constant ($g/cm^2/sec$)		Parabolic rate constant ($g^2/cm^4/sec$)	
	Experimental	Hagel	Experimental	Wagner
Fe–20Cr–25Ni	1.5×10^{-9}		1.6×10^{-11}	2.6×10^{-11}
Fe–20Cr–65Ni	3.3×10^{-9}		1.1×10^{-11}	2.5×10^{-11}
20Cr–80Ni	1.7×10^{-9}	3×10^{-10}	1.1×10^{-11}	2.5×10^{-11}
Nimonic 75	4.7×10^{-9}	to	3.2×10^{-11}	2.6×10^{-11}
Fe–25Cr–5Ni	2.0×10^{-10}	4×10^{-9}	3.9×10^{-11}	2.7×10^{-11}
Fe–25Cr–15Ni	4.2×10^{-9}		6.4×10^{-11}	2.6×10^{-11}
Fe–25Cr–20Ni	3.1×10^{-9}		2.9×10^{-11}	2.6×10^{-11}
Fe–25Cr–60Ni	6.2×10^{-9}		6.4×10^{-11}	2.6×10^{-11}
Fe–30Cr–5Ni	3.2×10^{-9}		1.8×10^{-11}	2.7×10^{-11}

where

$$(\Delta W/A) = \text{weight gain per unit surface area } (g/cm^2)$$

$$(k_p)^2 = \text{parabolic rate constant } (g^2/cm^4/sec)$$

$$k_v = \text{vaporization constant } (g/cm^2/sec)$$

determined values of the parabolic rate constants for the various alloys which were in excellent agreement with the values calculated using Wagner's analysis[29] (see Table IV). In addition, the values calculated for the vaporization constants fell within the range of values given by Hagel's[30] results for the evaporation of CrO_3 from Cr_2O_3 in oxygen atmospheres.

SUMMARY

The oxidation rates of iron–chromium–nickel alloys depend on both the nickel and the chromium contents. For a given chromium concentration in the alloys, increases in nickel content led to a progressive reduction in the oxidation rates.

For a given nickel concentration in the alloys, chromium contents of 0–10% Cr had very little effect on the oxidation rate, particularly for the iron-based alloys (Fig. 13). When chromium was present in these concentrations it was internally oxidized and the rate of oxidation was controlled by diffusion through the external scale phases, mainly $NiFe_2O_4$ and NiO. As the chromium content was increased from 10 to 20% Cr, an inner layer of chromic oxide was found beneath the main scale. The formation of the

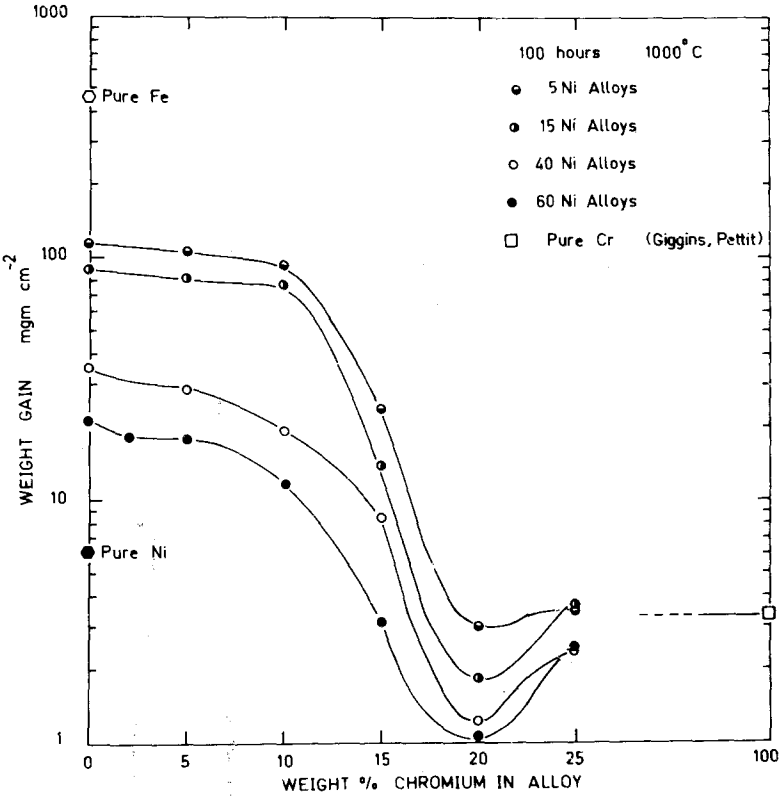

Fig. 13. The effect of chromium content on the oxidation rate of the ternary alloys as measured by the weight gains after 100 hr. of oxidation at 1000°C.

chromic oxide layer occurred earlier in the oxidation run and more completely over the specimen surface as the chromium content increased toward 20% Cr. Regardless of the nickel content, chromium levels of greater than 20% Cr led to the formation of a predominantly chromic oxide scale with the associated low diffusion rates through the scale and hence low oxidation rates, comparable with that of pure chromium.

The volatilization of CrO_3 from chromic oxide scales is now established as a feature of the oxidation of iron–chromium–nickel alloys at 1000°C and above, and it would appear that alloys protected only by chromic oxide scales are limited in their usefulness to temperatures below 1000°C.

ACKNOWLEDGMENTS

The work reported in this paper was conducted in the School of Metallurgy, University of New South Wales with the support of the Broken

Hill Proprietary Co. Ltd., Postgraduate Research Scholarship. The award of the scholarship and the provision of laboratory facilities by the head of the school are both gratefully acknowledged.

REFERENCES

1. J. E. Croll and G. R. Wallwork, *Oxid. Metals* **1**, 55 (1969).
2. H. J. Yearian, E. C. Randell, and T. A. Longo, *Corrosion* **12**, 515 t (1956).
3. G. L. Wulf, M. B. McGirr, and G. R. Wallwork, *Corr. Sci.* **9**, 739 (1969).
4. G. C. Wood and D. P. Whittle, *JISI* **202**, 979 (1964).
5. C. S. Tedmon, *J. Electrochem. Soc.* **114**, 788 (1967).
6. G. C. Wood, *Corr. Sci.* **2**, 255 (1961).
7. E. J. Felten, *J. Electrochem. Soc.* **108**, 490 (1961).
8. V. R. Howes, *Corr. Sci.* **8**, 221 (1968).
9. P. K. Footner, D. R. Holmes, and D. Mortimer, *Nature* **216**, 54 (1967).
10. G. C. Wood, *Corr. Sci.* **2**, 173 (1961).
11. G. C. Wood, T. Hodgkiess, and D. P. Whittle, *Corr. Sci.* **6**, 129 (1966).
12. G. C. Wood, *Oxid. Metals* **2**, 11 (1970).
13. B. Chattopadhyay and G. C. Wood, *Oxid. Metals* **2**, 373 (1970).
14. A. U. Seybolt, *J. Electrochem. Soc.* **107** 147 (1960).
15. G. C. Wood and T. Hodgkiess, *J. Electrochem. Soc.* **113**, 319 (1966).
16. R. A. Rapp, *Corrosion* **21**, 382 (1965).
17. R. T. Foley, *J. Electrochem. Soc.* **109**, 1202 (1962).
18. G. L. Wulf, T. J. Carter, and G. R. Wallwork, *Corr. Sci.* **9**, 689 (1969).
19. A. Dalvi, Research Report, Dept. of Met. and Mat. Sci., McMaster University, Hamilton, Ontario (1968).
20. G. S. Viktorovich, V. A. Gutin, and D. I. Lisovski, *Tsvetn. Metall.* **7**, 54 (1966).
21. H. J. Yearian, H. E. Boren, and R. E. Warr, *Corrosion* **12**, 561 t (1956).
22. J. E. Croll, Ph.D. Thesis, University of New South Wales, Australia (1971).
23. C. S. Giggins and F. S. Pettit, *Trans. AIME* **245**, 2495 (1969).
24. P. Schafmeister and R. Ergang, *Arch. Eisenhuttenw* **12**, 459 (1939).
25. C. H. M. Jenkins, E. H. Bucknall, C. R. Austin, and G. A. Mellor, *JISI* **136**, 187 (1937).
26. C. S. Tedmon, *J. Electrochem. Soc.* **113**, 766 (1966).
27. R. Kosak, Ph.D. Thesis, Ohio State University (1969).
28. G. R. Wallwork and A. Z. Hed, *Oxid. Metals* **3**, 171 (1971).
29. C. Wagner, "Atom Movements" A.S.M. Cleveland, Ohio (1951), p. 153.
30. W. C. Hagel, *Trans. ASM* **56**, 583 (1963).